UNIVERSITY OF TARTU

Faculty of Science and Technology

Institute of Physics

Muhammad Usama Jamal

Energy transfer processes in solid solutions $Zn_xCd_{1-x}WO_4$

Master's Thesis

(30 ECTS in Materials Science and Technology)

Supervisors: Dr. Vitali Nagirnõi

Dr. Nataliya Krutyak

Laboratory of Physics of Ionic Crystals

Institute of Physics

University of Tartu

Tartu 2022

Energy transfer processes in solid solutions $Zn_xCd_{1-x}WO_4$

Abstract

The present research is devoted to the investigation of energy transfer processes in solid solutions $Zn_xCd_{1-x}WO_4$. Its motivation is based on previous studies of intrinsic scintillating materials with excitonic emission, which showed that the scintillation yield of solid solutions (mixed crystals) may be higher than that in their constituents due to the changes in energy transfer processes, induced by structural disorder in mixed crystals. The main research method was time-resolved luminescence spectroscopy under photoexcitation and electron beam irradiation. The studies did not reveal enhancement of light yield in the studied solid solutions, however, important information on the processes of exciton creation was obtained.

The measurements of emission spectra of $Zn_xCd_{1-x}WO_4$ solid solutions at low (12.2 and 78 K) and room temperature (RT) revealed the displacement in the position of the emission band towards lower wavelengths with changing Zn concentration (x value). The shifts were irregular, especially in the sample with low Zn content (x=0-0.3). In addition, it was also observed that the emission band is broader in samples with intermediate Zn content (x=0.5). The reason of the irregular shift in the position of the emission band with increasing x value was clarified by the studies of emission decay kinetics. Two decay components were revealed in the studied samples: τ_1= 15 μs characteristic of $CdWO_4$ and τ_2= 28 μs known for $ZnWO_4$. Decay curves were measured in the region 400 nm to 650 nm with a step of 25 nm for the whole series $Zn_xCd_{1-x}WO_4$ (x=0-1), and integrated spectra of both components were obtained by fixing τ_1 and τ_2 values for all compounds. The integrated emission spectra showed that even a minimal concentration of Zn in the solid solution makes the contributions of both components in the total emission comparable. Based on this fact it was concluded that excitons are created preferentially near Zn cation in $Zn_xCd_{1-x}WO_4$ solid solutions.

In excitation spectra, a gradual low-energy shift of the excitation band edge was observed in solid solutions by increasing Zn content at 12.5 K and RT in accordance with the fact that the bandgap of $ZnWO_4$ (4.6 eV) is smaller than that in $CdWO_4$ (4.98 eV). Cathodoluminescence studies also confirmed that excitons formed in the process of recombination of electron-hole pairs are mainly created near the zinc site. In thermostimulated luminescence (TSL) curves, two main broad peaks were observed around 90 K and 140 K, which indicates the presence of two different traps in the studied crystals. A near-linear dependency on Zn concentration was

observed for the intensity of the peaks, indicating that also the trapping and recombination of trapped charge carriers takes place preferentially near Zn cations.

Keywords: energy transfer, luminescence, scintillation mechanism, excitons, spectroscopy, photoluminescence, decay kinetics, thermostimulated luminescence, scintillators.

CERCS: P260 Condensed matter: electronic structure, electrical, magnetic, and optical properties, superconductors, magnetic resonance, relaxation, spectroscopy; T151 Optical materials.

Energia ülekande protsessid tahketes lahustes $Zn_xCd_{1-x}WO_4$

Käesolev töö on pühendatud energia ülekande protsesside uurimisele tahketes lahustes $Zn_xCd_{1-x}WO_4$. Töö motivatsioon põhineb varasematel eksitonkiirgusega stsintillaatormaterjalide uuringute tulemustel, mis näitasid, et tahkete lahuste stsintillatsiooni saagis võib olla suurem, kui lahust moodustavatel koostisosadel eraldi. Käesoleva töö põhiliseks uuringumeetodiks oli aeglahutusega spektroskoopia foto- ja elektronergastusel. Need uuringud ei tuvastanud tahkete lahuste valgussaagise suurenemist, kuid siiski aitasid saada olulist informatsiooni eksitonide teke kohta.

$Zn_xCd_{1-x}WO_4$ tahkete lahuste kiirgusspektrite uurimine madalal (12.2 and 78 K) ja toa temperatuuril ilmutasid lahuste kiirgusribade nihet väiksemate lainepikkuste poole Zn kontsentratsiooni (x väärtuse) suurenedes. Nihe on ebakorrapärane, eriti madalate tsingi sisalduste puhul (x=0-0.3). Kiirgusriba on kõige laiem keskmise tsingi kontsentratsiooni (x=0.5) puhul. Sellise ebaregulaarse nihke põhjusi tuvastati tahkete lahuste kiirguse kustumiskineetika uurimisel. Nimelt, kõikide lahuste kiirguse kustumises leiti kaks komponenti kustumisajaga τ_1= 15 µs ja τ_2= 28 µs, mis on iseloomulikud vastavalt $CdWO_4$ ja $ZnWO_4$ kristallidele. Kiirguse kustumiskõverad olid salvestatud lainepikkuste 400 kuni 600 nm sammuga 25 nm, ning mõlema komponentide jaoks saadi integreeritud kiirguse spektreid, fikseerides τ_1 and τ_2 väärtusi. Saadud spektrid näitasid, et Zn lisandamine $CdWO_4$ kristalli isegi minimaalsel kontsentratsioonil teeb mõlema komponendi panuse materjali kiirguses võrreldavaks. Selle põhjal tõestasime, et tahketes $Zn_xCd_{1-x}WO_4$ lahustes tekivad eksitonid eelistatavalt tsingi võresõlme läheduses.

Samuti leiti, et tahkete lahuste kiirguse ergastusspektri äär nihkub järg-järguliselt tsingi kontsentratsiooni suurenedes. Selline nihe on heas vastavuses keelutsooni kitsenemisega, kuna selle laius on 4.98 eV $CdWO_4$-s ja 4.6 eV $ZnWO_4$-s. Katoodluminestsentsi eksperimendid kinnitasid, et eksitonid, mis tekkivad tahketes lahustes elektron-aukude rekombinatsiooni käigus moodustuvad samuti eelistatult tsingi võresõlme läheduses. Kaks põhilist laia piiki tuvastati kiritatud kristallide termostimuleeritud luminestsentsis, mis viitavad sellele, et tahketes lahustes domineerivad kaks põhilist laengukandjate lõksu. Nende piikide intensiivsuse peaaegu lineaarne sõltuvus tsingi kontsentratsioonist tõestab, et ka laengukandjate lõksustumine ja rekombinatsioon toimub tsingi võresõlme läheduses.

Võtmesõnad: energia ülekanne, luminestsents, stsintillatsiooni mehhanism, eksitonid, spektroskoopia, fotoluminestsents, kustumiskineetika, termostimuleeritud luminestsents, stsintillaatorid.

CERCS: P260 Tahke aine: elektrooniline struktuur, elektrilised, magneetilised ja optilised omadused, ülijuhtivus, magnetresonants, spektroskoopia; T151 Optilised materjalid.

Contents

Abbreviations

e-h	Electron-Hole
E_g	Energy Gap
PL	Photoluminescence
CL	Cathodoluminescence
RT	Room Temperature
XRF	X-ray Fluorescence
UV-VIS	Ultraviolet-Visible
VUV	Vacuum Ultraviolet
SR	Synchrotron Radiation
STE	Self-trapped exciton
PMT	Photomultiplier Tube
CT	Computed Tomography
PET	Positron Emission Tomography

1. Introduction

The conversion of energy is an important phenomenon for many radiation detection systems and has a wide application in many fields such as medical imaging, homeland security, high energy physics (HEP) calorimetry, industrial control, and oil drilling exploration. When energetic radiation interacts with a material, ionization takes place in the material and as a result, free charge carriers are produced that are either detected by direct or indirect detection techniques. For direct detection, the generated charge carriers are collected by a semi-conductor which gives rise to an electric pulse. This technique is especially used in gamma spectrometry. However, the direct detection technique is less favorable in terms of cost as it requires cryogenic conditions. Another possible way of detection is to expose the ionizing radiations on a material that can absorb higher energy and transform the absorbed radiations into lower energy by emitting photons. This kind of detection is called indirect detection which is performed by the scintillators.

Energy transportation is a significant process of any scintillation mechanism. Scintillation is the conversion of X-rays, γ rays, or such high-energy particles as neutrons, accelerated charged particles like protons, electrons, and heavy ions into UV-visible photons, i.e. a flash of light. Materials capable of performing such conversion are called scintillators. The UV-visible light photon is further converted into an electrical signal by a photodetector. A pictorial representation of the process is shown in ***Figure 1***. This energy transformation is carried out in three steps: conversion, energy transfer, and luminescence. In the first conversion step, the incoming radiation interacts with the scintillating material (usually wide bandgap ionic compound) in the following ways: photoelectric effect, Compton scattering, and pair production. Photoelectric effect and Compton scattering phenomena are dominant for low to medium energy range, i.e. less than a few hundred keV for photoelectric effect and from hundreds of keV to 8000 keV for Compton scattering, while pair production occurs when the energy of the incident photon is higher than the twice of the electron resting mass i.e. 1.022 MeV. At the end of this stage, the produced hot electrons and deep holes gradually thermalize at the edges of the conduction and valence band. The whole conversion process occurs within a time range of a few picoseconds. In the energy transfer step, the created e-h pair migrate through the host material to the emission centers and transfer the energy to that center. This energy transfer process can be delayed due to the repeatedly trapping of charge carriers at the trapping level generated because of lattice defects. This delay in the energy transfer process causes afterglow and increases the decay time of the scintillator emission up

to microseconds or milliseconds. The e-h pair from the luminescence center recombines radiatively and releases lower energy radiation in the form of luminescence in the final stage [1].

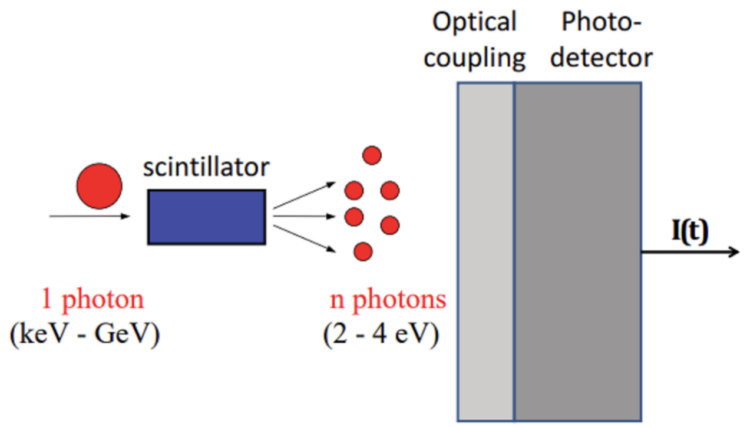

Figure 1: Illustration of the radiation detection process occurs in scintillating material-based detectors. [1]

The scintillating materials exist in different states, i.e. solid, liquid, or gaseous. Among all these states solid forms of scintillators are widely used. Solid forms are further divided mainly into two subcategories, i.e. organic and inorganic scintillators. In the current era, inorganic scintillators are most popular in terms of their practical applications and had an estimated market value of $350 million in 2015. Since there is constant up-gradation in detector technologies and ionizing radiation systems and also continuous development and optimization in materials synthesis methods, the scintillators are still in a focal point of research and development activities [2].

Based on the chemical formula, solid state scintillators are divided into different families, i.e. halide and oxide scintillators. The present thesis focuses only on a type of oxide scintillator and the research is performed on a solid solution of two different divalent cation tungstate, i.e. $CdWO_4$ and $ZnWO_4$. The transition metal tungstates MWO_4 gain the interest of researchers because of their intrinsic luminescent property. As in an intrinsic emission material, the luminescence takes place by the electron transfer among the tungsten (W^{6+}) and oxygen (O^{2-}) ions within the WO_4 or WO_6 complexes of the crystal [3]. Therefore, it does not require doping and defects which ultimately affect the homogeneity and quality of the crystal.

Divalent cation tungstates are well known for their scintillation properties and a lot of work is done to understand the properties of single crystals. Nowadays scientists are paying more attention to mixed crystals ($A_{1-x}B_xWO_4$) to get the combined properties of two different compounds in a single form [4] [5]. For example, a compound of good scintillation properties merges up with a compound of good mechanical properties.

The main aim of the work is:

- To investigate the photostimulated and thermostimulated characteristics of the $Zn_xCd_{1-x}WO_4$ that reveal the effect of zinc substitution on energy transfer mechanism of mixed crystal.

In order to achieve the goal set, the following subtasks were fulfilled:

- A complete series of $Zn_xCd_{1-x}WO_4$ solid solutions (x=0-1) was synthesized by spontaneous crystallization technique by other research group.
- Emission and excitation spectra were measured at the Photoluminescence setup and Synchrotron station (Synchrotron measurements were performed by the supervisor). The measurements were performed at 12 K, 78 K, and room temperature.
- Decay kinetics studies were performed from emission wavelength 400 nm to 650 nm with a step of 25 nm to draw integrated emission spectra of each component.
- Cathodoluminescence spectra were measured at 5.5 K.
- Thermostimulated luminescence studies were performed in the range of 6 – 200 K.

2. Literature review

2.1 Scintillation mechanism

As mentioned earlier, scintillation is the transformation of energy that occurs by following a multistep mechanism. In this section, the whole scintillation mechanism that occurs in an ionic crystal is discussed briefly.

The scintillation mechanism is entirely based on the relaxation of electronic excitation. The simplest way to explain this relaxation process is the scheme proposed by A. Vasil'ev [6]. This scheme consists of the material's band structure in which different stages of the electronic relaxation are described, from the primary excitation to the final stage of light emission.

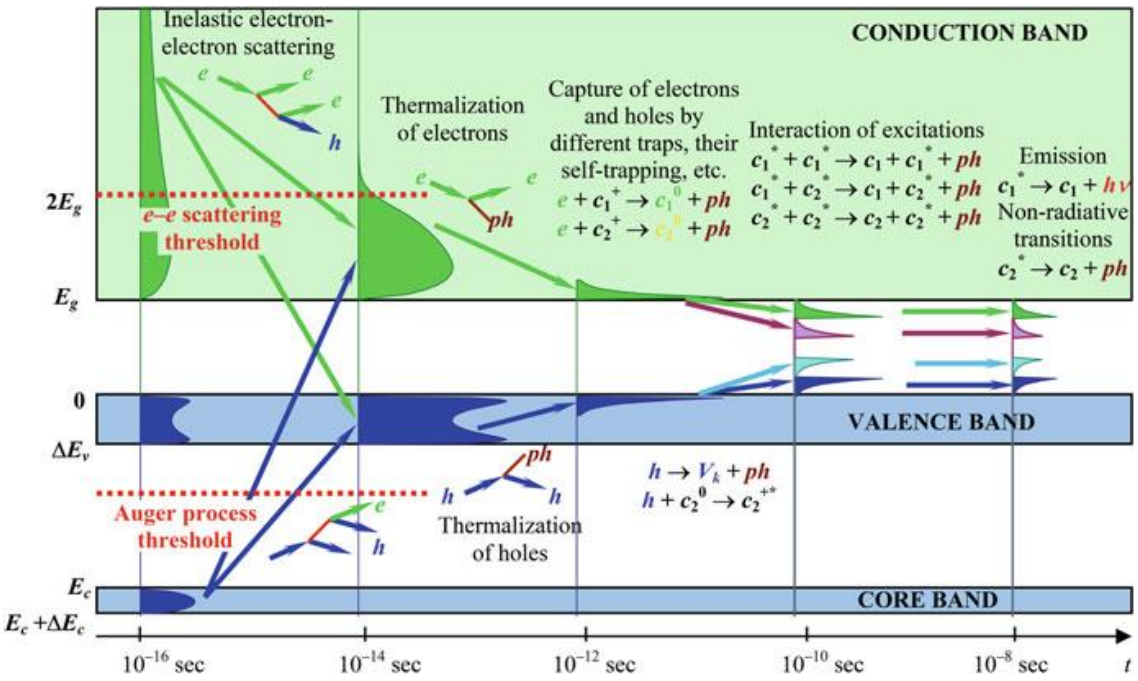

Figure 2: Scheme of relaxation of electronic excitations in an intrinsic scintillator. e = electrons, h=holes, ph = phonons, hν = photons, Vk = self-trapped holes, cn = ionic centers with charge n. [7]

A general scheme of the scintillation mechanism is shown in ***Figure 2*** where various electronic energy bands are illustrated. The core band is displayed with the maximum energy E_c and bandwidth ΔE_c. The valence band has the top energy $E_v = 0$ and bandwidth ΔE_v and is

separated from the conduction band by the forbidden bandgap of width E_g. There are five main stages of the relaxation mechanism.

The first stage begins with creating primary excitation as the result of an interaction between ionizing radiation and the material. Highly energetic radiation creates deep holes *h* in the inner-core band and a hot electron *e* in the conduction band. Within a very short time (10^{-16} - 10^{-14} s), multiplication of electronic excitation takes place, and a large number of secondary electrons and holes are produced in the conduction and valence band through the inelastic electron-electron scattering and Auger process. This stage ends once all the electrons' energy in the conduction band becomes $< 2E_g$ and all holes accumulate at the valence band after the Auger process.

In the second stage, thermalization of electronic excitation occurs, and phonons are produced. The thermalization process decreases the kinetic energy of electrons and holes, thus the electrons move to the bottom of the conduction band and holes occupy the top of the valence band.

In the third stage, the localization of electronic excitation occurs due to an interaction with different trapping levels present in the crystal. These traps are created because of the defects and impurities present in the crystals. Besides trapping defects and impurity centers, excitations can also be self-trapped in the crystal lattice in the form of self-trapped excitons, and self-trapped holes (V_k centers) by emitting phonons. The localization of excitation can be accompanied by disturbing the alignment of atoms in a crystal lattice. Relaxed excitations can also migrate in the crystal and transfer their energy to emission centers. In the end, electrons and holes are recombined together either radiatively and/or non-radiatively.

2.2 Performance parameters of scintillating materials

Scintillating material performance and application area are determined based on several parameters. Generally, these parameters depend on the chemical composition of the material but they can also vary due to the crystal structures, growing techniques, impurities, etc. Some important parameters determining the quality of a scintillator and suitability for various applications are discussed here [8] [9].

2.2.1 Scintillation yield

Scintillation yield indicates the number of photons created due to the interaction between ionizing radiation and scintillation material, and it is usually expressed as the number of

photons per MeV or keV (ph/MeV or ph/keV). The conversion ratio of high-energy quanta into a bundle of low-energy photons is also described as scintillation efficiency and it depends on several elements like the energy bandgap of the material (E_g), the energy of incoming radiation (E), and quantum efficiencies of different stages (S and Q). The scintillation efficiency of a material can be calculated as,

$$N(\text{photon}) = \frac{E}{\beta \, . Eg} S \, . Q$$

Where, $\beta.E_g$ is the average energy required for the creation of one thermalized electron-hole pair, S is the energy transfer efficiency and Q is luminescence quantum yield.

2.2.2 Decay time / Time response

Decay time corresponds to the time required by emitted photons to reach e^{-1} of their highest number. It is also defined as the time needed by the material to be ready for responding to another photon of ionizing radiation. Scintillation decay time ranges from hundreds of picoseconds up to milliseconds or more based on the trapping levels and the energy transportation mechanism of the material. Scintillator operating speed plays a crucial role in predicting the application field of the material. According to the time response, scintillating materials are divided into two categories: i) fast scintillators ii) slow scintillators. Fast ones are used in such applications where a fast counting rate of quanta is required (usually < 1 μs) and the detector can distinguish the energy deposition per quantum and show a good time resolution. Slow scintillators are used in the integration regime where the distinction of quanta is not required and decay time can be longer until the afterglow starts affecting the detection.

2.2.3 Density

Density plays a vital role in selecting scintillating materials, because it directly impacts the detector volume and performance. Dense material reduces the interaction area for high energy radiation and electrons and it also decreases the photon diffusion of the emitted light, which improves segmentation and spatial resolution of the detector. Moreover, a high-density material occupies less volume. It has more atoms to interact with the incoming radiation, which eventually increases the stopping power of the scintillator and reduces the size of the detector. Following such advantages of high-density scintillating materials, inorganic crystalline compounds are synthesized that have density $\rho > 8$ g cm^{-3} like lead tungstate $PbWO_4$ crystals (8.28 g cm^{-3}) and lutetium aluminum perovskite (8.34 g cm^{-3}) [9].

2.2.4 Energy Resolution

Energy resolution refers to the inherent property of scintillating materials to differentiate between particles of variable energies. A suitable detector responds proportionally to the energy deposited by the particle in the scintillating material in a wide range.

2.2.5 Scintillation Wavelength

It is the wavelength of photons that are emitted due to the recombination of electrons and holes at the last stage of the scintillation mechanism. This wavelength is important because the detectors used for converting photons into electrons work efficiently in selected wavelength ranges. Therefore, it is worthy to have such material that can emit photons in that spectral region suitable for detectors.

2.2.6 Radiation Damage

Ionizing radiations can create defects in exposed scintillating materials. These defects may be responsible for color centers in the crystals due to which the material may lose its transparency. Moreover, severe damage might decrease the light yield of the scintillator. Therefore, stability under ionizing radiation is essential for scintillating materials, especially for the detectors used in well-logging, space, and high energy physics experiments. The strength of materials depends on crystal intrinsic features but also on crystal growing technique. If a method favors the growth of less defected crystals, the material will have better stability against ionizing radiation.

2.2.7 Thermal, chemical, and mechanical stability

Thermal stability indicates the stability of scintillation parameters like scintillation wavelength, decay time, or scintillation yield with temperature changes. Thermal stability is important for scintillators used in such application fields as oil well logging, where temperature changes tens of degrees during operation. Sometimes a difference of 10 °C can affect the scintillation performance significantly. Chemical stability is of real importance concerning the lifetime of the scintillation detector, some scintillating materials show excellent scintillating properties but due to their hygroscopic nature, extra packaging is required which makes them unsuitable materials for the compact detectors.

2.2.8 Cost

The cost factor gains fundamental importance in that application fields, where one particular detector contains several tons of scintillating materials like in high energy calorimetry, or in

common application fields, where the usage of the detector is extensive, like medical imaging and homeland security. The cost of scintillating materials depends on various factors such as desired purity of raw material, production yield, production technique, and required atmospheric conditions.

2.2.9 Material form

The size and shape of scintillating materials have significant importance regarding their scintillation properties. Based on the demand from various application fields, scintillating crystals are synthesized in different forms and sizes ranging from a few mm up to several tens of cm. Different techniques are employed to produce different forms of materials, i.e. thin films, fibers, ceramics, or crystalline powders.

3. Application fields of scintillators

The application of scintillating materials varies according to their performance parameters. Some application fields where scintillating materials are commonly used are discussed below.

3.1 Medical diagnostics

The use of scintillators for medical science was discovered more than a century ago by Wilhelm Röntgen [10]. During his experiments with a cathode ray tube, he came to know that there is invisible radiation of very high energy that can penetrate through the tube and be absorbed by high-density materials, i.e. BaPt(CN)4 which further emits visible light. This chemical compound allowed the discovery of unknown radiation named X-ray. Subsequently, a series of experiments were performed to assess the penetration power of this radiation, and different objects were exposed to radiation. During placing the object Röntgen realized that it can also pass through the tissues but is absorbed by the bones of his hand. To demonstrate this discovery to the world, Röntgen performed an X-ray scan of his wife's hand and published that discovery. After publishing his observations, it brought a breakthrough in the field of medical science.

The scintillating properties of BaPt(CN)4 were not up to the mark to produce a high-resolution X-ray image. Therefore, the search for appropriate scintillating material became the center of attention for the scientist that possesses the required properties. Soon $CdWO_4$ and ZnS were discovered as good scintillating materials because of their good luminescence property. Since the discovery of X-rays, research is being performed on new scintillating materials and detection systems. The field of X-ray radiology has acquired such a level of

advancement that an inside 3D image of the human body can be produced easily by using the computed tomography (CT) technique. Moreover, scintillator-based detectors are also used in nuclear imaging techniques such as Positron Emission Tomography or Single Photon Emission computed tomography. In the mentioned tomography techniques, a radioactive chemical compound (radiotracers) is injected into the bloodstream, this molecule targets specifically the tumor area leading to cell uptake. This technique is used to detect the gamma photons emitted due to the radioactive disintegration of the radiotracers that provide information about the location of the tumor. Moreover, 3D images of tumors can also be produced by such detectors, which helps in diagnosing the severity of the disease [9].

3.2 Safety system

The second common application of scintillating materials is in the field of homeland security. In this field, scintillator-based detectors are mainly used for the following purposes: i) scanning the items of luggage and passengers at airports, train stations, etc., ii) detecting explosive materials, and iii) searching fissile materials remotely.

The scanning of the luggage and passengers is performed very similarly to the X-ray imaging technique performed in a CT scanner. However, in this case, very high-energy radiation is required that can pass through the luggage. A detector of good spatial resolution is also needed that can form a high-resolution image of each item inside the luggage based on the densities of the items.

The demand for controlling the transportation of explosive materials surged right after the 2001 attack in the USA. For detecting explosives, the nuclear radiation detection techniques seem quite promising. Hence, the majority of nuclei such as C, O, N, Cl, and S are vital for identifying explosive materials emit gamma quanta of the energy range higher than 4 MeV under neutron irradiation, which is enough for ionizing scintillating materials [9]. Consequently, scintillating materials-based detectors are a good option for this application. Moreover, nuclear radiation detectors comprising scintillating materials also allow the detection of fissile materials that are commonly used in nuclear weapons. Fissile materials emit gamma photons during fission reactions, which strongly signals their existence. The method of remote detection of fissile materials was deployed in compliance with the Nunn-Lugar Act to control the spread of nuclear weapons [9]. This method is also helpful to prevent the smuggling of fissile materials.

3.3 High energy physics

The application of scintillating materials can also be seen in particle physics (high energy physics). This branch of physics provides information about the fundamental building block of matter by the collisions of highly accelerated particles. As a result of collisions, many secondary particles are produced that are analyzed and detected to extract information about the matter. A significant fraction of these particles is detected by a scintillating material-based device known as a calorimeter. The factor that differentiates this application from other applications is the energy difference of particles. The scintillating materials used in high-energy calorimetry interact with the particles of energies up to TeV. Several tons of scintillating materials are usually used to acquire enough stopping power of materials that can deal with such high energy.

4. Scintillating materials

Solid scintillating materials are classified into two classes, doped and undoped scintillators. Doped scintillators are those in which a trivial amount of impurities such as thallium (Tl^{+}), silver (Ag^{+}), telluride (Te^{2+}), divalent or trivalent rear earth ions are doped as an activator into the scintillating material. Activators usually substitute for cations in the crystal lattice and create localized energy levels between the bandgap of the host material. Dopants are used either to enhance the light output, decrease the afterglow, or change the emission wavelength of the crystal. Undoped or self-activated scintillators are intrinsic luminescence materials that show good scintillation properties without doping any activator ion. Oxides scintillators such as $Bi_4Ge_3O_{12}$ (BGO) and metal tungstate MWO_4 (M= Zn, Cd, Mg, Sr, Ca, Ba) are examples of self-activated scintillators which show excellent scintillation properties without doping of activator ions [11].

4.1 Cadmium Tungstate ($CdWO_4$)

$CdWO_4$ is a member of the divalent cations tungstate family and has a long history as a scintillating material. The luminescence properties of this material were first investigated by Kroger [12]. Because of its good scintillating properties such as high density, large effective atomic number, wide emission band in the visible region, sufficiently short decay time, and high light output, $CdWO_4$ is a well-known scintillating material. It is widely used in different fields such as X-ray tomography, slow neutron detection, and dosimetry [13] [14] [15].

$CdWO_4$ has a monoclinic wolframite-type crystal structure (space group P2/c) and unit-cell parameters: a = 5.0289 Å, b = 5.8596 Å, c = 5.0715 Å, β = 91.519° [16]. The unit cell of

$CdWO_4$ has two formula units. ***Figure 3*** represents the crystal structure of $CdWO_4$. In the crystal lattice, each W atom is surrounded by six oxygen atoms in approximately octahedral coordination. The crystal of $CdWO_4$ contains two distinct oxygen atoms shown as O1 and O2 in ***Figure 3***. The first type of oxygen atom, O1 is linked to two Cd atoms with a longer bond length of 2.273 and 2.414 Å, and one W atom with a shorter bond distance of 1.785 Å. While the second type of oxygen O2 links to two different tungsten atoms with bond lengths (1.910 Å and 2.145 Å) and a Cd atom with a Cd–O2 bond length of 2.198 Å.

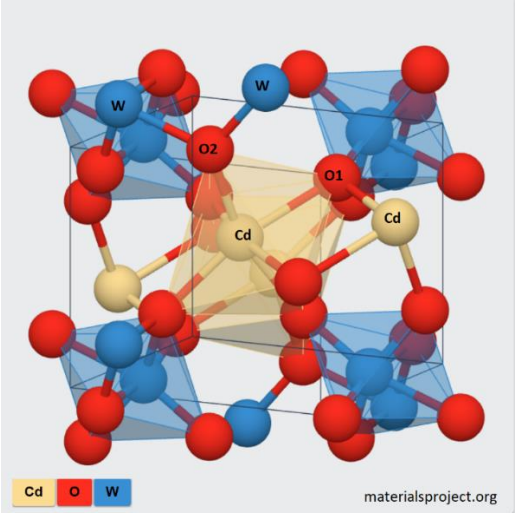

Figure 3: Crystal structure of cadmium tungstate, $CdWO_4$: Cd-yellow spheres; W-blue spheres; O-red spheres. A unit cell is outlined. [17]

Electronic band structure studies of $CdWO_4$ show that oxygen 2p states mainly occupy the top of the valence band, while the main constituent of the bottom of the conduction band is tungsten 5d states [18] [17]. A pictorial representation of the density of states is also shown in ***Figure 4.*** The intrinsic luminescence $CdWO_4$, a wide band peaking at 495 nm, is due to the charge transfer from tungsten 5d to oxygen 2p states forming excitons that are self-trapped at the WO_6^{6-} complexes. The energy band gap of $CdWO_4$ is reported 4.94 eV by R. Laasner [19].

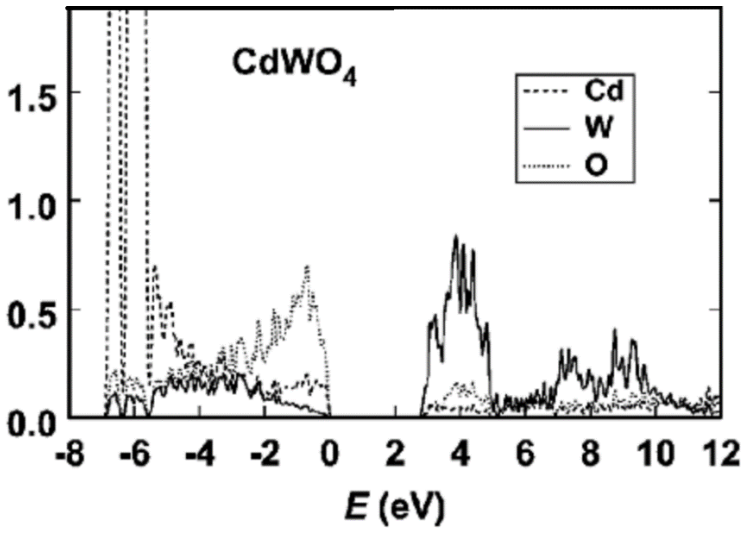

Figure 4: Partial density-of-states for conduction and valence bands of $CdWO_4$ crystal. Cd, W, and O states are plotted with dashed, solid, and dotted lines. [18]

***Table 1: Properties of $CdWO_4$ crystal** [9].*

Properties	**$CdWO_4$**
Structure	Monoclinic
Cleavage	(010)
Density	7.99 g/cm^3
Light output (%) relative to NaI	38
Z_{eff}	64.2
Decay time (µs)	15
Emission band	495 nm
Afterglow	0.005 (3)
Conversion factor (electrons / eV)	0.01

4.2 Zinc Tungstate ($ZnWO_4$)

$ZnWO_4$ is a self-activated scintillating material and its luminescence properties were discovered in the mid of last century [12]. $ZnWO_4$ is considered a good scintillating material due to its promising scintillating and physical properties like emission wavelength, high density, high scintillation efficiency, short decay time, low afterglow, good mechanical properties, inexpensiveness, non-hygroscopic and non-toxic nature [20] [21] [22] [23] [24].

Based on such properties $ZnWO_4$ is a suitable material for different applications such as X-ray computed tomography (XCT) [20], γ-spectroscopy [21], search for double beta (2β) decay [25], and cryogenic dark matter experiments [26].

$ZnWO_4$ crystals are present in a monoclinic wolframite type structure and represent P2/c crystal symmetry with the following unit-cell parameters: a = 4.69263 Å, b = 5.72129 Å, c = 4.92805 Å, β= 90.6321° [27]. The crystal structure of $ZnWO_4$ consists of two formula units in each primitive cell. The crystal structure of $ZnWO_4$ has two different oxygen atoms O1 and O2 as shown in ***Figure 5***, the differentiation is based on their bonding with the nearest atom. O1 atoms are directly bonded with two tungsten atoms, and one zinc atom, whilst O2 atoms are linked with two zinc atoms and one tungsten atom. Each zinc and tungsten atom is surrounded by six oxygen atoms and forms ZnO_6 and WO_6 octahedral coordination [27]. The energy bandgap of the $ZnWO_4$ crystal is reported 4.6 eV by V.N. Kolobanov [28].

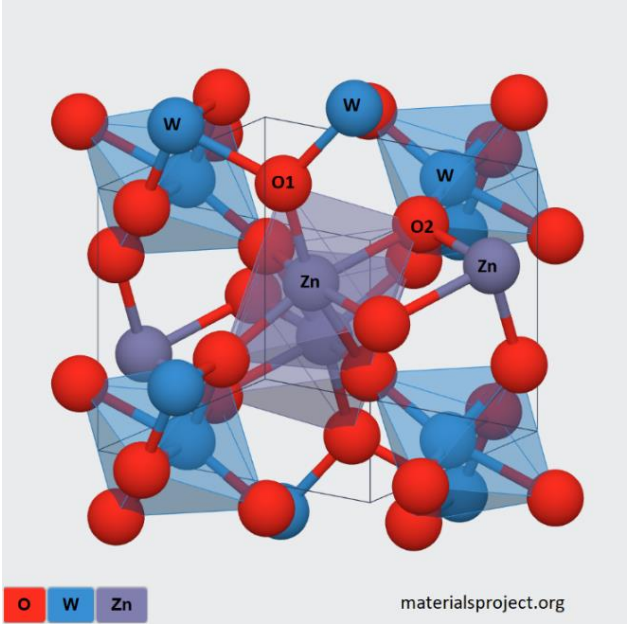

Figure 5: Crystal structure of zinc tungstate, $ZnWO_4$: Zn - purple spheres; W - blue spheres; O - red spheres. A unit cell is outlined. [27]

Table 2: Properties of $ZnWO_4$ crystal *[20] [23] [9].*

Properties	**$ZnWO_4$**
Structure	Monoclinic
Cleavage	(010)
Density	7.87 g/cm^3
Light output (%) relative to NaI	28
Z_{eff}	62.5
Decay time (µs)	25
Emission band	480 nm
Afterglow (@ 3 ms)	<0.001

5. Solid solution of $ZnWO_4$ and $CdWO_4$

A solid solution is a mixture of different crystalline materials crystallized in a single crystalline solid or crystal lattice. The solid solution synthesis technique is becoming famous day by day. It allows the research community to tune and control the structure of crystalline materials by incorporating chemical compounds of different chemical natures. There could be several benefits of mixing two compounds such as cost reduction, increment in light output or scintillation yield, moderate decay time, imparting mechanical strength to the material, and giving required stopping power to the materials by combining materials of different densities, etc.

$CdWO_4$ and $ZnWO_4$ crystallize in the same type of structure and space group as already discussed previously. Moreover, their cell parameters and ionic radius are also close, allowing growing a complete series of solid solutions [29]. The intentions to mix $ZnWO_4$ in $CdWO_4$ are to i) obtain better crystal structure at an intermediate concentration (x=0.5) where thermalization length decreases and more electron and holes are transferred to luminescence center, consequently light yield of the crystal increases, as observed in the case of $Zn_xMg_{1-x}WO_4$ [30] ii) curb environmental pollution without compromising the scintillation properties of the material. Challenges connected to $CdWO_4$ are i) it contains inherent macro defects (pores and cracks) that occur due to the gas-forming impurities incorporated from the melt

during production, and ii) release of CdO in gaseous form, which pollute the environment. On the other hand, $ZnWO_4$ has some advantages, it can be grown of high quality without any inclusion by a modified Czochralski method [31] and it does not affect the environment like Cd. But there are some limitations associated with $ZnWO_4$ such as relatively low light output compares to $CdWO_4$ and coloration. By mixing these two materials, the advantageous properties of pure components can be combined together.

6. Methods and Instruments

6.1 Photoluminescence

The photoluminescence studies were performed in the Laboratory of Ionic Crystals, Institute of Physics, University of Tartu. The measurements were performed on an experimental setup customized for experiments in the UV-Vis (1.5–6 eV) range. In this UV-Vis setup, two different types of lamps are used as excitation sources: a 400-watt deuterium discharge lamp DDS-400 is used to measure excitation and emission spectra, however, PerkinElmer 150 W xenon pulsed flash lamp (1 µs) is particularly used for decay kinetics. Both excitation sources are used in combination with a primary double-quartz prism monochromator DMR-4. The samples were placed in a Janis VPF-800 liquid nitrogen cryostat (78-800 K) either by conductive silver glue or screw tightened copper clip. Emission spectra were recorded with the help of an ARC Spectra Pro 308i Czerny-Turner type grating monochromator equipped with a photomultiplier tube H8259-01. Excitation and emission spectra were measured at room temperature and at 78 K. A temperature controller LakeShore 335 is used to monitor temperature and control crystal heating. Different glass filters provided by SCHOTT were used to get rid of second orders of excitation and emission in the secondary monochromator. The experimental setup was operated by using a software named LabView. A pictorial representation can be seen in ***Figure 6.***

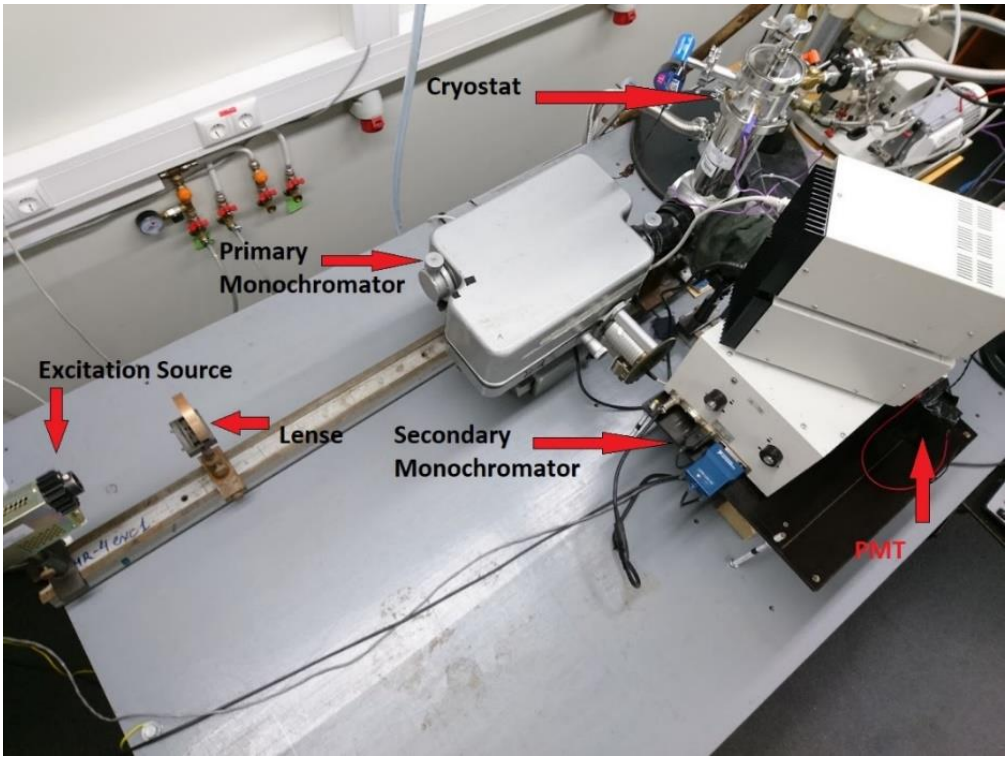

Figure 6: Photoluminescence spectroscopy instrument present at Institute of Physics, University of Tartu.

6.2 Cathodoluminescence and Thermostimulated luminescence

Cathodoluminescence and TSL studies were performed on a customized dual-channel setup equipped with a helium cryostat, which allows for performing studies at a temperature range 5-400 K. Channel 1 allowed emission spectra measurements in the UV-VUV region 4 – 11 eV, i.e. a Johnson-Onaka double monochromator equipped with Hamamatsu PMT R6836 detector, while another channel employed for the Vis-UV region 1.8 – 6 eV, based on an ARC SpectraPro 2300i grating monochromator equipped with different detectors. An electron gun (Kimball Physics EGG-3101) of energy up to 10 keV is used as an excitation source, which can be operated in both steady and pulse (5 kHz, 10 ns) modes. This electron gun produces a beam of spot size 0.5 mm^2 and has a penetration depth of 0.5 µm, which was focused at the surface of the sample. The steady mode of the electron gun is used to irradiate the sample, after that TSL spectra were recorded for an integrated emission or at a selected emission wavelength range with the help of PMT. TSL curves were recorded at a heating rate of 6 K/min.

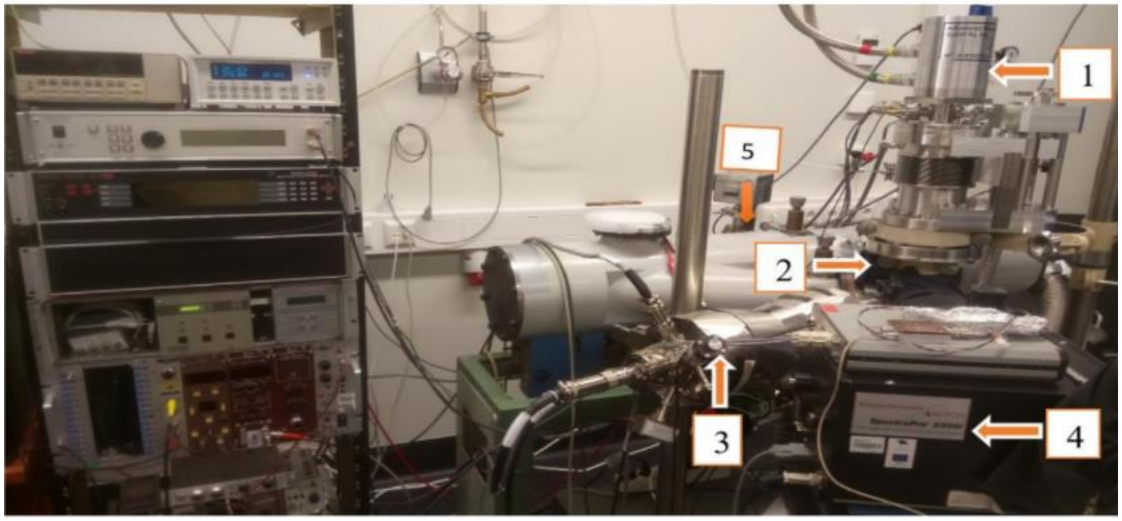

Figure 7: Cathodoluminescence setup. The components of the CL setup are designated by numbers on the photo.

(1) a closed cycle vacuum cryostat (Advanced Research Systems); (2) Vacuum chamber ≈ 10 −7 Torr; (3) An electron gun (EGG-3101 Kimball Physics); (4) ARC Spectra Pro 2300i spectrometer for the UV-visible range; (5) a home-built VUV monochromator.

7. Samples preparation

Zinc-cadmium tungstate crystals ($Zn_xCd_{1-x}WO_4$) were grown by spontaneous crystallization of a solution of oxides ZnO, CdO, and WO_4 in a melt of sodium chloride. The composition of the crystals varied according to the metals cationic group with a step of 0.1 from x = 0 to x = 1.0. As initial charge components, the indicated metal oxides of the especially pure grade were used and sodium chloride was of chemical grade. To obtain crystals of required stoichiometry, the content of oxide components of the charge was calculated from the ratio:

$$x\ ZnO + (1-x)\ CdO + WO_3 \rightarrow Zn_xCd_{1-x}WO_4$$

Oxides in a given ratio were thoroughly mixed with a chloride content of 25.0% wt. in all cases. The crystals were grown in aluminum oxide crucibles of a volume of 30 ml in a temperature-controlled oven. The oven was heated up to 900 °C at a rate of 6 °C / min and held at 900 °C for 2Hr for melt homogenization. Then temperature was decreased in three stages. In the first stage, the melt was cool down from 900 to 880 °C at a rate of 0.1 °C / min, in the second stage it was cool down from 880 to 860 C at 0.3 °C /min, and in the last, from 860 to 800 °C at a rate of 0.8 °C / min. Then the heating was turned off and allowed it to cool down up to room temperature.

The resulting crystals were separated from the solvent by boiling the crucibles with their contents in water. After separation, the crystals were carefully washed with distilled water and dried.

Figure 8: A series of ZnxCd1-xWO₄ crystals used in measurements.

The composition determination was also performed at our institute by the supervisor. The X-ray fluorescence (XRF) technique was employed for determining the ratios of the Zn and Cd in the mixed crystal. The results are shown in the ***Table 3*** in terms of percentages. Although, the composition assigned by the provider was considered for the measurements because the results we obtained were from a single crystal of cross-section of around 0.5 mm, however in each sample holder consists of more crystals whose composition differs a bit.

Table 3: *Percentages of each component obtained by XRF.*

Sample	**Zn Content (%)**	**Cd Content (%)**
$Zn_{0.1}Cd_{0.9}WO_4$	8.7	91.2
$Zn_{0.2}Cd_{0.8}WO_4$	22.1	77.9
$Zn_{0.3}Cd_{0.7}WO_4$	31.3	68.7
$Zn_{0.5}Cd_{0.5}WO_4$	56.8	43.2
$Zn_{0.6}Cd_{0.4}WO_4$	75.7	24.3
$Zn_{0.7}Cd_{0.3}WO_4$	80.2	18.7
$Zn_{0.8}Cd_{0.2}WO_4$	91.5	8.5
$Zn_{0.9}Cd_{0.1}WO_4$	84.8	15.2

8. Results and Discussion

8.1 Excitation and Emission

The measurements of emission and excitation spectra of the synthesized samples were performed at the P66 synchrotron station, DESY, Hamburg, and at the laboratory photoluminescence setup in Tartu. The measurements at the synchrotron station at room temperature and 12 K were carried out by the supervisor and treated by myself, while liquid nitrogen temperature measurements at the photoluminescence setup were carried out and analyzed by myself. In addition, RT measurements of the complete series of emission spectra were also performed at the photoluminescence set up using a pulsed Xenon flash lamp (1 µs). In each experiment, the measurement conditions were kept exactly the same for all samples to study the effect of changing Zn concentration on the luminescence properties of the material. As the position of the maximum of the emission band in $CdWO_4$ and $ZnWO_4$ is 495 and 480 nm, respectively, one could expect a gradual displacement of the emission band in their solid solutions $Zn_xCd_{1-x}WO_4$, when the concentration ratios of cations are changed.

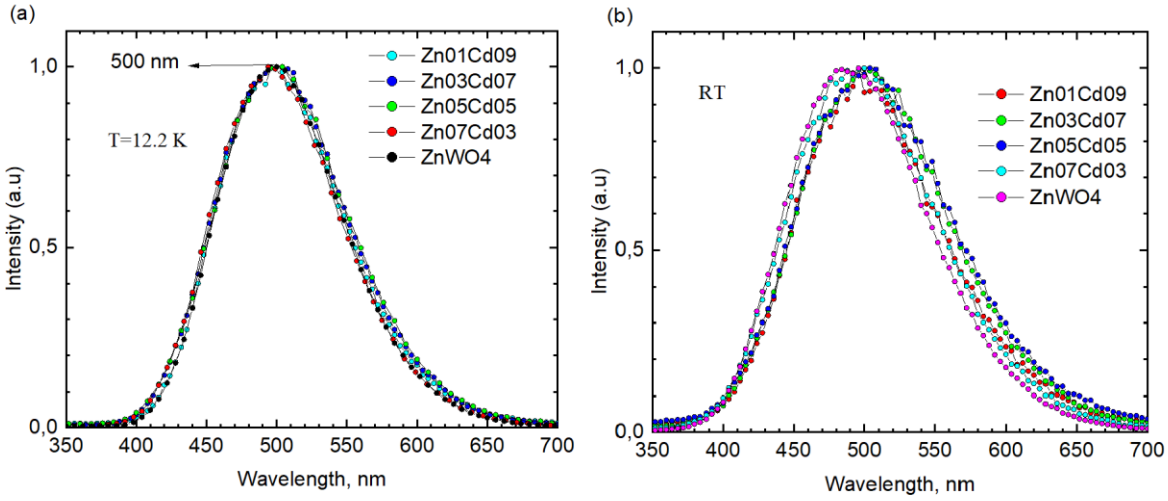

Figure 9: Emission spectra measured under excitation 4.2 eV at the P66 synchrotron station at 12.2 K (a) and RT (b).

Figure 9a shows the emission spectra of $Zn_xCd_{1-x}WO_4$ for x = 0.1, 0.3, 0.5, 0.7, and 1, measured at 12.2 K under synchrotron irradiation at 4.2 eV. As shown in Figure, in samples x= 0.1, 0.3, and 0.5 the position of the emission band moved gradually to a higher wavelength with increasing the concentration, while the samples containing higher Zn showed emission band position at lower wavelengths but at random positions. The emission

band FWHM showed a maximum value at x=0.5, there was a linear relationship observed between the x value and the emission band FWHM at lower concentrations of Zn (x=0.1-0.5), however, higher values of x showed an inverse relation, more clearly visible in ***Figure 10.***

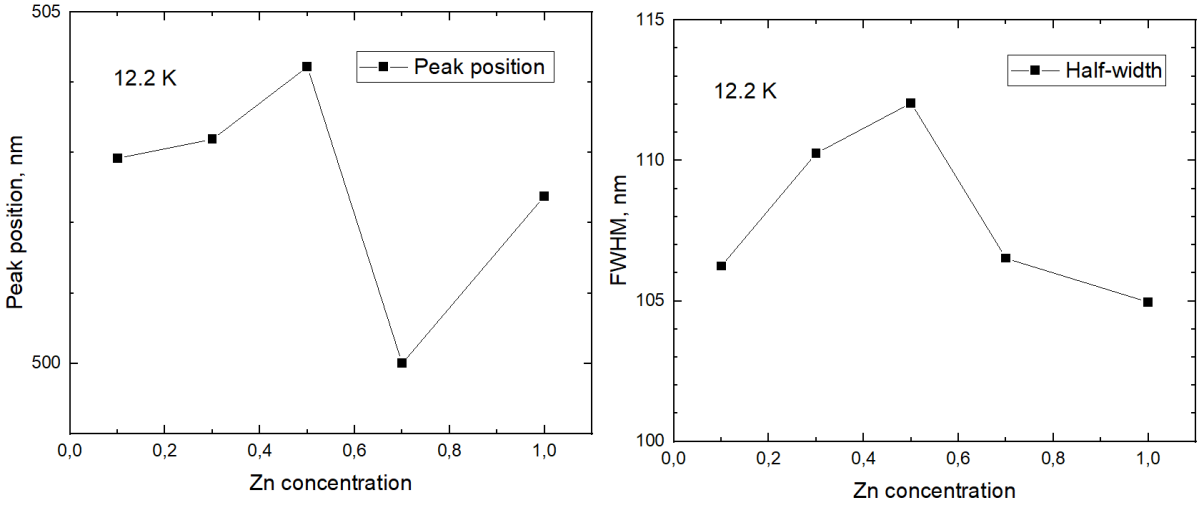

Figure 10: Graphical representation of peak positions and FWHM of emission bands obtained at 12.2 K under synchrotron irradiation.

At room temperature, the displacement of the emission band with the increase of Zn concentration is better visible ***(see Figure 11)***, whereas a small shift in the band maximum is observed between the samples having low zinc concentrations x=0.1, 0.3, 0.5 and the samples having a high Zn content x=0.7 and x=1. The samples with low Zn content give maximum emission near 500 nm, while other showed maximum emission near 480 nm, which can be seen in ***Figure 9b.***

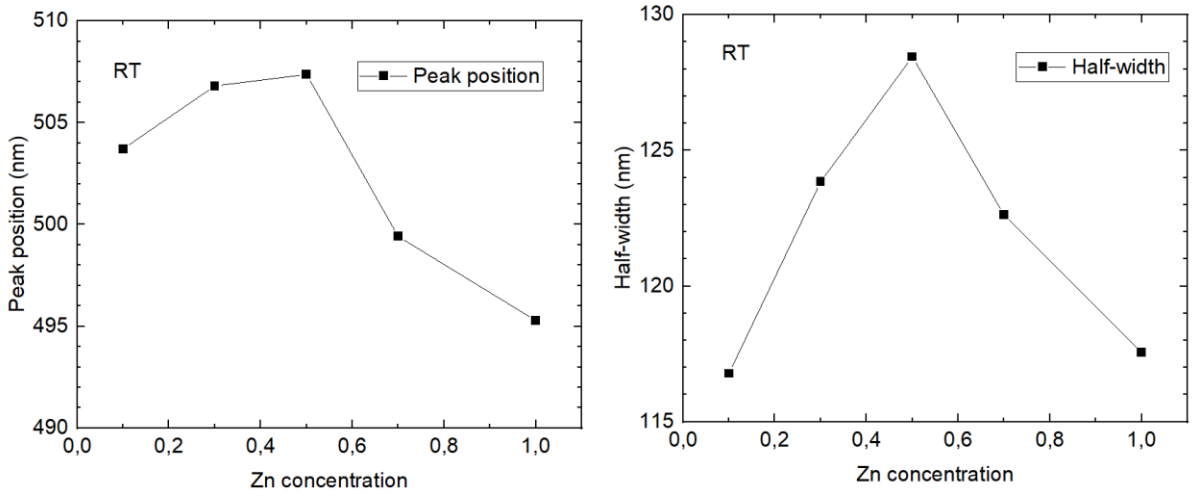

Figure 11: Graphical representation of peak positions and FWHM of emission bands obtained at RT under synchrotron irradiation.

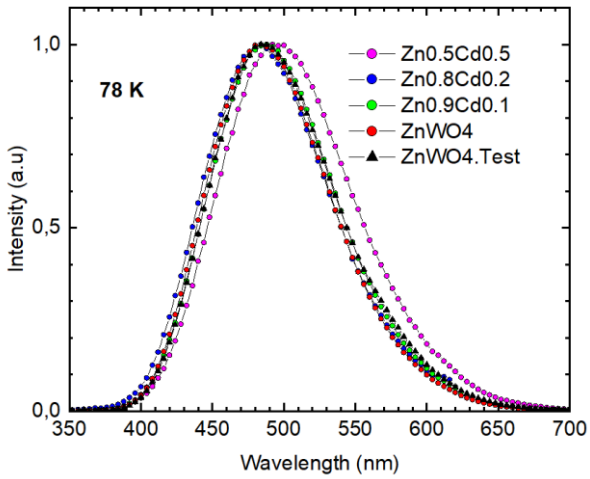

Figure 12: Emission spectra measured under excitation 4.2 eV at the Photoluminescence setup at 78 K.

As both the position and half-width of the emission band of $ZnWO_4$ deviated from the monotonous dependences of these emission parameters on x value, the emission spectra were also measured at the photoluminescence setup at the Institute of Physics at 78 K for the samples with high Zn concentration and at RT for the whole set of available samples. In addition, the emission band characteristics were studied for a high quality $ZnWO_4$ crystal grown at the Wigner Research Centre, Budapest, Hungary. At 78 K, an irregular shift in the band edge is observed in all samples with x=0.5, 0.8, 0.9, 1, and a reference crystal. Despite

an obvious short-wavelength shift of the emission band is observed at transition from x=0.5 to x=0.8, an opposite shift takes place for x=0.9 and 1 (see ***Figure 12 and 13***).

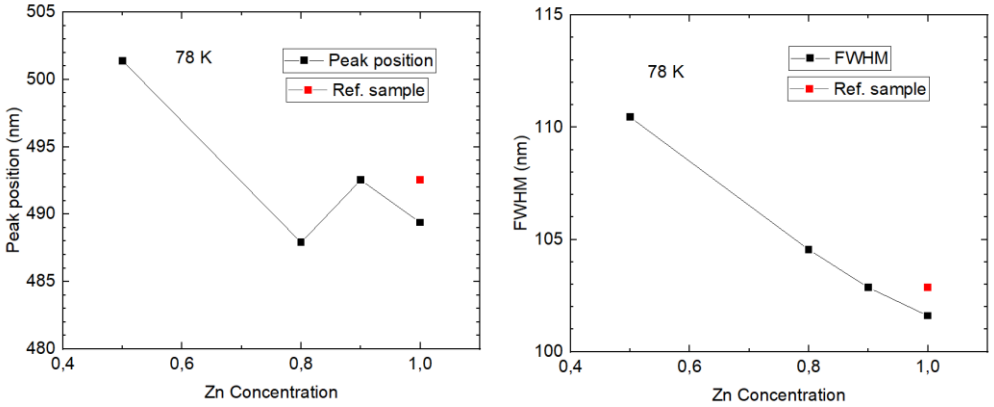

Figure 13: Graphical representation of peak positions and FWHM of emission bands obtained at 78 K at Photoluminescence setup.

Figure 14 shows emission spectra of a complete series of $Zn_xCd_{1-x}WO_4$ (x=0-1) measured at RT by using a 1-μs Xenon flash lamp. One can see from the ***Figure 15***, that while the emission band FWHM shows the main tendency to be bigger at average x values, the change in the band positions is relatively random. The reason of such behaviour will be clarified below in the section devoted to the emission decay kinetics studies.

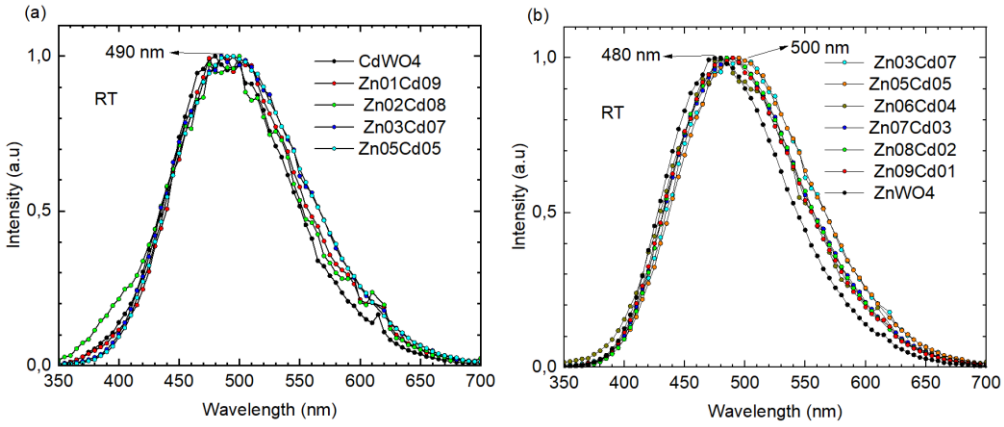

Figure 14: Emission spectra measured under (1-μs) pulse excitation 4.2 eV at the Photoluminescence setup at RT.

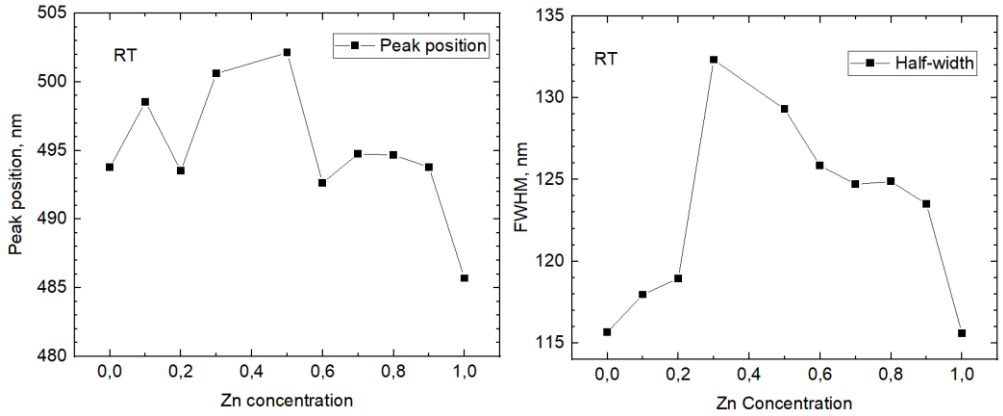

Figure 15: Graphical representation of peak positions and FWHM of emission bands obtained at RT at Photoluminescence setup.

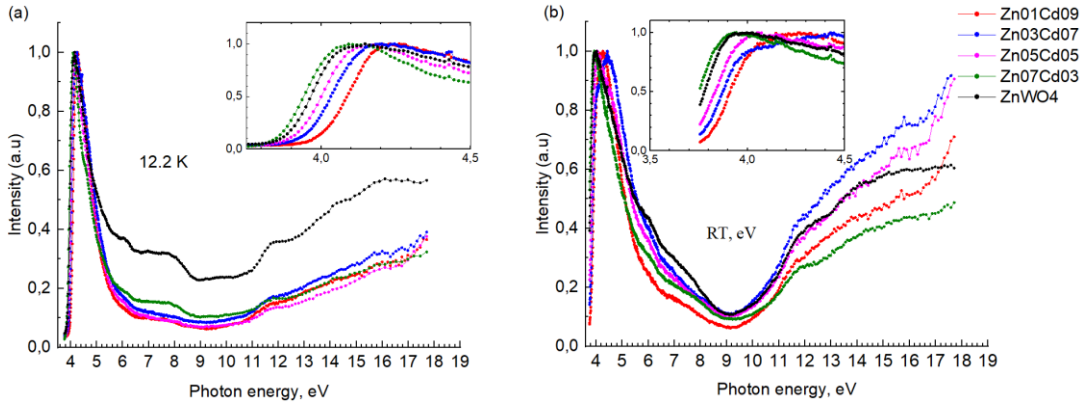

Figure 16: Excitation spectra measured at emission wavelength 500 nm at the P66 synchrotron station at 12.2 K (a) and RT (b).

Figures 16a and b show the excitation spectra of $Zn_xCd_{1-x}WO_4$ with x = 0.1, 0.3, 0.5, 0.7, and 1, measured under synchrotron irradiation at 12.2 K and RT. At 12.2 K, the excitation of the $Zn_{0.1}Cd_{0.9}WO_4$ sample starts at approximately 4 eV and then the onset gradually moves to the low-energy side with an increasing x value except $ZnWO_4$, where an opposite shift in the excitation edge was observed. At RT, the onset of the excitation spectrum of $Zn_{0.1}Cd_{0.9}WO_4$ moves to 3.85 eV due to electron-phonon interaction, but the low-energy shift of the onset with increasing x is also clearly visible, only the onset of $ZnWO_4$ spectrum appeared at unexpected position. Otherwise the photoluminescence excitation spectra measured at low temperature and RT under synchrotron irradiation show similar well-pronounced dependence of the onset of the excitation spectrum on zinc concentration. To verify the irregular displacement of the emission excitation edge of $ZnWO_4$, excitation measurements were also

performed at photoluminescence setup at 78 K, and in addition, a high quality $ZnWO_4$ crystal was also measured as a reference sample. ***Figure 17*** shows the luminescence excitation spectra of the $Zn_xCd_{1-x}WO_4$ mixed crystals for x=0.5, 0.7, 0.8, 1, and a pure $ZnWO_4$ single crystal, measured at 78 K within the excitation energy range of 3.5 eV to 6 eV for the 500-nm emission. An apparent gradual shift in the excitation edge from 3.95 eV to 3.85 eV corresponding to an increase in the zinc concentration is also observed, as it was noticed in synchrotron measurements. The photoluminescence measurements confirmed the non-monotonous displacement of the excitation spectrum edge for the sample with x=1, however, the onset of the reference $ZnWO_4$ sample appeared at expected energy. The unexpected onset position of the samples having x=0.9 and 1 ($ZnWO_4$) can be related to structural imperfections and surface influence in the studied small-size crystals. To verify this suggestion, additional Raman shift and XRD studies are planned for future, however, some conclusions concerning the quality of the crystal surface may be done based on already recorded excitation spectra. Namely, it is observed that all samples except the reference sample of a pure $ZnWO_4$ single crystal show a decrease in excitation efficiency at the energies above 4.2 eV. Such decrease is attributed to charge carrier trapping and subsequent energy losses on surface defects present in the synthesized small-size samples. The reference sample shows no such efficiency decrease due to a high quality of its surface.

The shift of the excitation edge in $Zn_xCd_{1-x}WO_4$ is in good correspondence with a small difference in the bandgap width of $CdWO_4$ and $ZnWO_4$. The displacement of the excitation edge from higher to lower energy indicates the reduction of the energy bandgap due to increasing Zn concentration which means that Zn^{2+} has a stronger polarization effect on $[WO_4]^{2-}$ than Cd^{2+}, owing to the reduction in the energy transfer between O and W. In its turn, the behavior of the emission spectrum is not that unambiguous. In particular, no gradual shift in the emission band is observed and the peak position and band width change unevenly. In an attempt to understand the reason of such behavior, we studied time-resolved emission spectra for the whole set of samples.

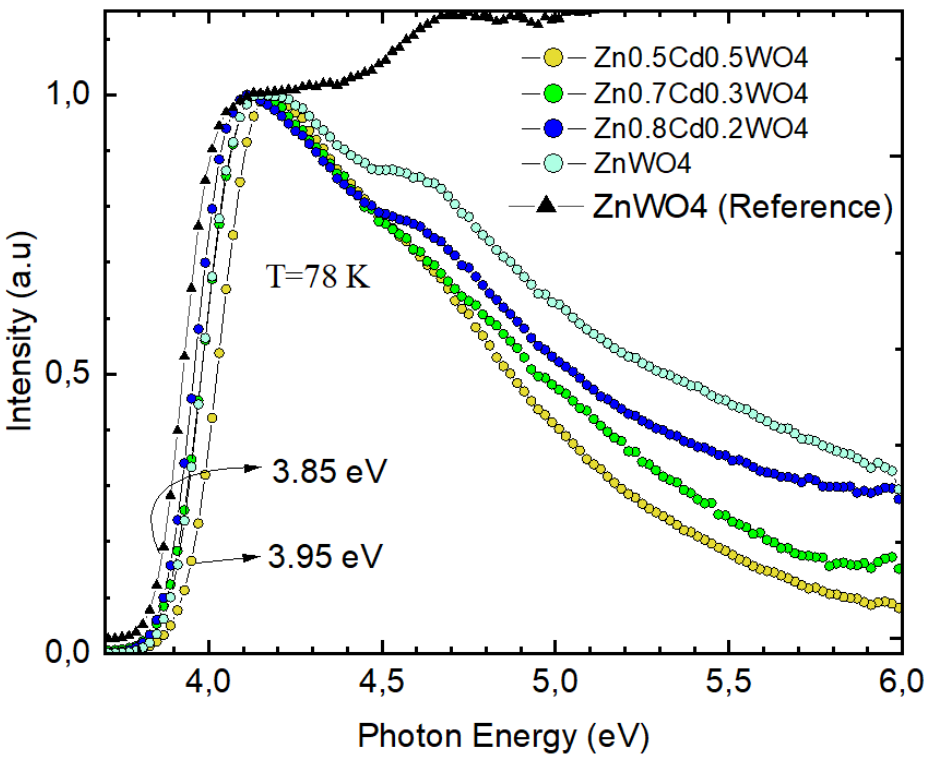

Figure 17: Excitation spectra measured at emission wavelength 500 nm at the Photoluminescence setup at 78 K.

8.2 Decay kinetics studies

Time-resolved emission spectra of a complete series of $Zn_xCd_{1-x}WO_4$ (x = 0 – 1.0) were measured in the wavelength range from 400 nm to 650 nm with a step of 25 nm. All the measurements were performed with 1-μs pulses of excitation energy of 4.2 eV. In each spectral point, a decay curve was recorded and decomposed in single exponential components. The integrated intensity of each component was calculated as $I=A_i\tau_i$, where A_i is initial intensity and τ_i is decay time of a corresponding decay component. In good agreement with the published data [9], two components were distinguished in the decay curves with τ_1=15 μs characteristic of $CdWO_4$ excitons and 28 μs known for $ZnWO_4$ excitons, both decay times at RT. In the cases of intermediate x values, when the separation in two components was not reliable, the values τ_1 and τ_2 were fixed in decay curve decomposition to give an approximate contribution from the faster and slower component.

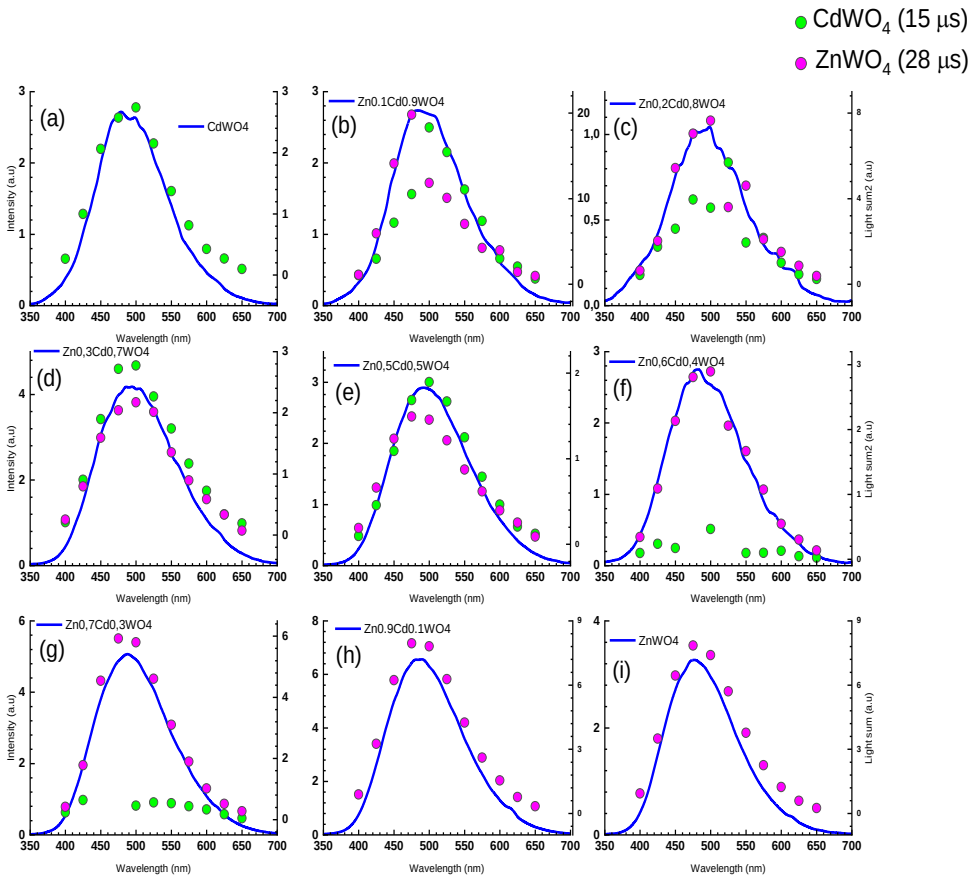

Figure 18: Time-resolved emission spectra (dots) compared to integrated spectra of $Zn_xCd_{1-x}WO_4$ samples. Magenta and green dots represent the components with decay time 28 and 15 μs, respectively.

Figure 18 represents the integrated emission spectra and light sum spectra of two exponential components obtained from the decay kinetics studies performed for all the samples. Unexpectedly, there is no gradual change of the contribution of $ZnWO_4$ related excitons with τ_2=28 μs and $CdWO_4$ related excitons with τ_1=15 μs into the total emission with changing x value. According to the obtained spectra, the decay kinetics of $CdWO_4$ is represented by one decay component τ_1. However, already at the lowest concentrations of Zn (x=0.1, 0.2 and 0.3) the intensities of both τ_1 and τ_2 components are comparable, see ***Figures 18b, c and d.*** At the higher Zn content starting from x=0.6, the intensity of the $CdWO_4$ related component becomes very low, as compared to $ZnWO_4$ component, and τ_1 disappears completely at x=0.9.

It may be concluded from such behaviour of the two decay components, that excitations are relax preferentially close to zinc cation in the studied mixed crystals. Even minimal zinc

content in the sample shows a noticeable effect on the emission band, which is visible in ***Figure 18b***. Based on this, it can be assumed that exciton formation is highly favorable on WO_6 anion complexes having zinc in their surrounding in mixed crystals, and because of this, a gradual shift in the emission band position with changing x value cannot be seen in $Zn_xCd_{1-x}WO_4$ solid solutions.

8.3 Cathodoluminescence studies

To support this observation cathodoluminescence studies were also performed. Two samples of low zinc content and two of high zinc content, i.e. $Zn_xCd_{1-x}WO_4$ (x=0.2, 0.3, 0.7, 0.8), were selected for the measurements. The samples were excited by electron beam of 10 keV, which created hot holes in the valence band and hot electrons in the conduction band. ***Figure 19*** illustrates the CL spectra measured at 5.5 K, showing an insignificant random of the emission band position for all samples. However, all samples showed maximum emission close to 483 nm, which indicates that the e-h pair created by the irradiation converts in STE near Zn sites and emits photons characteristic of the $ZnWO_4$ emission in accord with the conclusion made on the basis of emission decay kinetics studies.

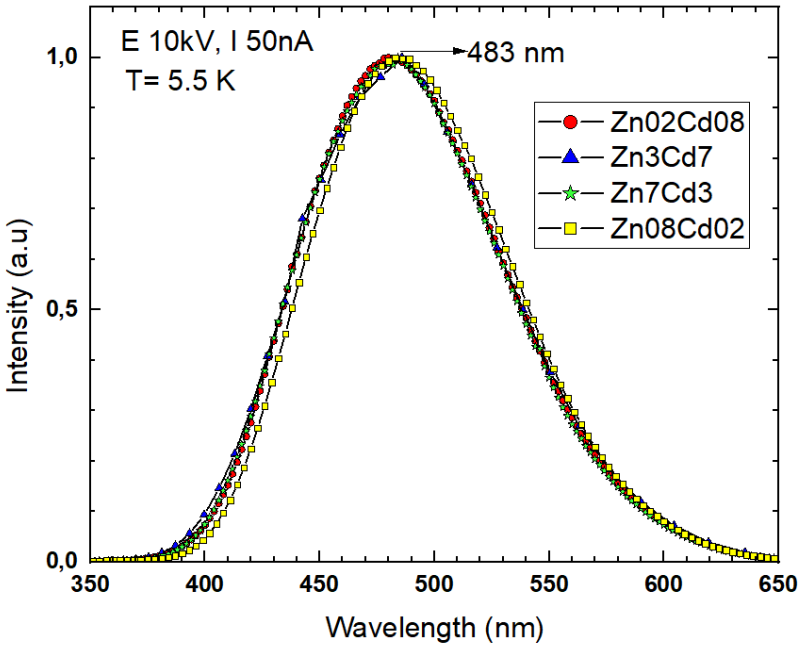

Figure 19: Emission spectra measured under excitation 10 keV at the Cathodoluminescence setup at 5.5 K.

8.4 Thermostimulated Luminescence

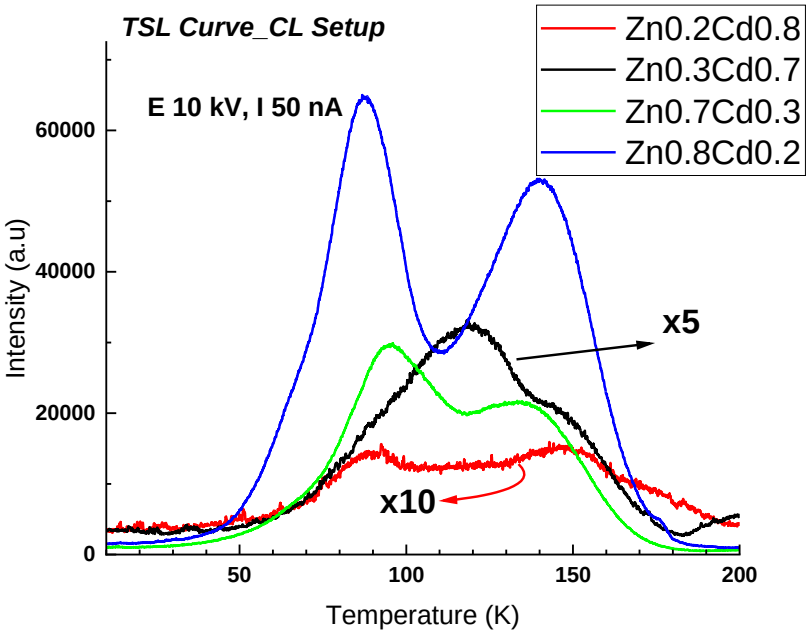

Figure 20: TSL curve measured at Cathodoluminescence setup in a temperature range 6-200 K. Sample were irradiated for 30 minutes under 10 keV electron energy.

Figure 20 shows the TSL curves of $Zn_xCd_{1-x}WO_4$ (x= 0.2, 0.3, 0.7, 0.8) samples measured at the cathodoluminescence setup. The samples were irradiated for 30 minutes by 10 keV electron beam at 5 K and heated up at a rate of 6 K/min by a heat controller. Two main broad peaks were observed in all samples near 90 K and 140 K, corresponding to two different charge carrier traps in the material. The traces of an additional peak can be detected in crystals with low Zn content. The intensity of the two main peaks showed near linear relation with the concentration of zinc in the samples, which indicates that the corresponding charge carrier traps could be located close to the Zn site. Same near linear dependency was also observed for $Zn_xCd_{1-x}WO_4$ (x= 0.3, 0.5, 0.7, 0.8) samples measured at the photoluminescence setup where samples were irradiated for 30 minutes under 5.7 eV excitation energy at 78 K, the first peak is partially bleached at irradiation at 78 K which can be seen in ***Figure 21.*** In addition, TSL spectra were measured at temperatures around the TSL peaks for all samples measured at CL setup (***Figures 22a, b, c and d)***. One can see, that the TSL peaks near 100 K correspond to the emission wavelength of 490 nm while higher temperature peaks have emission wavelength of 480 nm which can be seen clearly in ***Figure 22d***. Based on the obtained spectra, it can be assumed that the traps are located near the zinc states which

showing emission of 480 nm, and also somewhere between cadmium and zinc site which are showing emission of 490 nm.

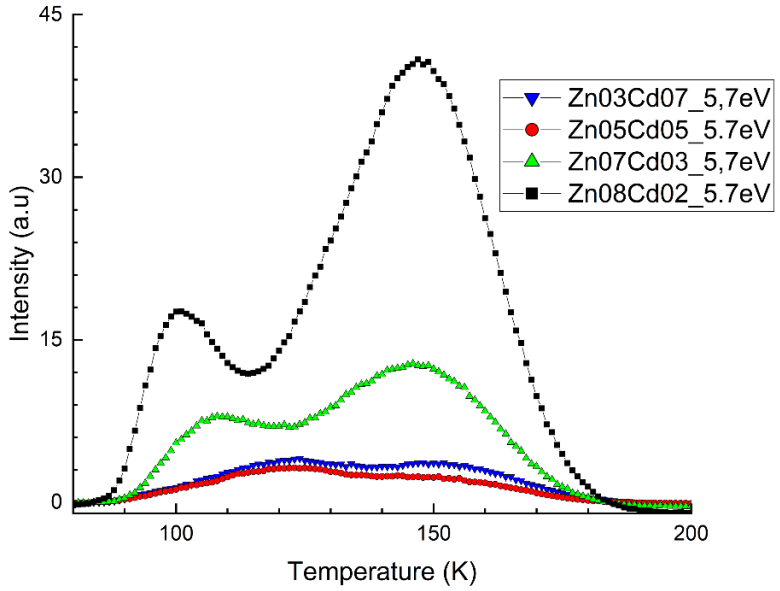

Figure 21: TSL curve measured at Photoluminescence setup in a temperature range 78-200 K. Sample were irradiated for 30 minutes under 5.7 eV excitation energy.

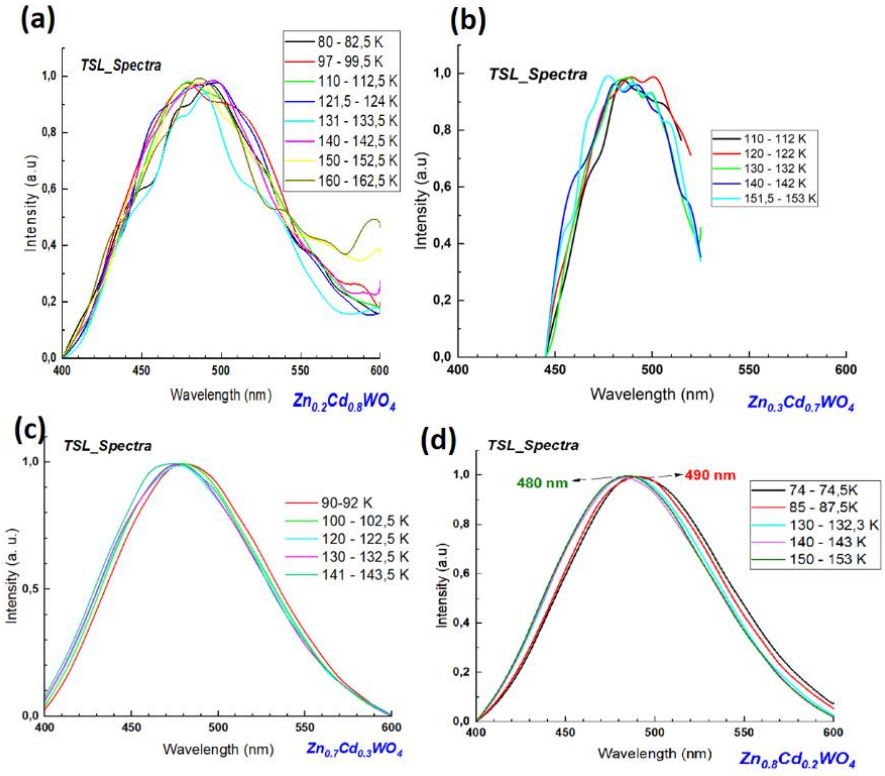

Figure 22: TSL spectra of two main peaks of TSL curve measured at Cathodoluminescence setup by using PMT detector.

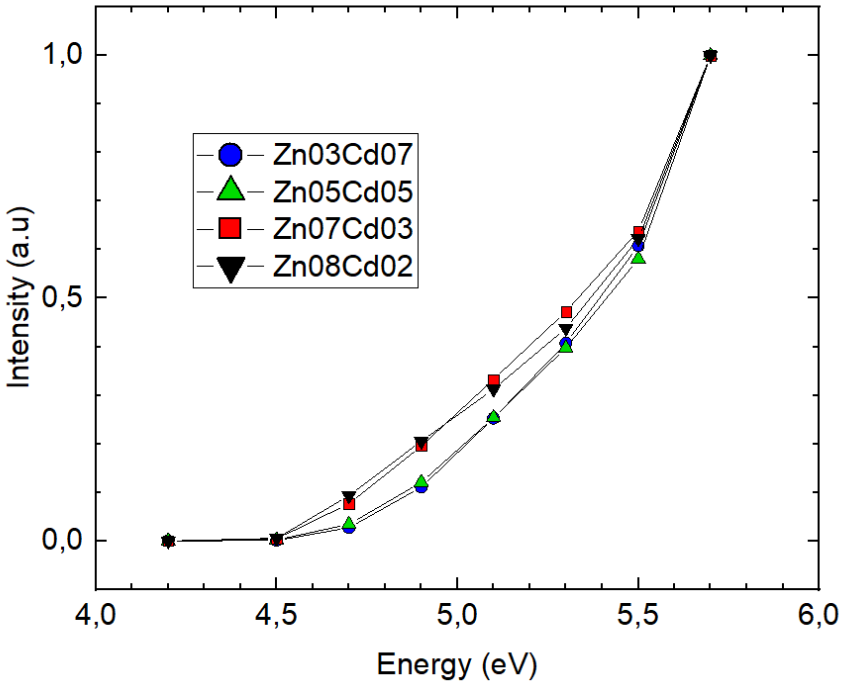

Figure 23: TSL excitation spectra of samples $Zn_xCd_{1-x}WO_4$ x= 0.3, 0.5, 0.7 0.8 irradiated for half hour at energies 4.3 eV to 5.7 eV at 78 K.

Figure 23 shows the TSL excitation spectra of the samples with Zn content x=0.3, 0.5, 0.7 and 0.8. Each point in the spectra was obtained upon the irradiation the sample for 30 minutes by UV light of selected energies 4.2, 4.5, 4.7, 4.9, 5.2, 5.5 and 5.7 eV at 78 K, followed by recording the TSL curve at heating the sample up to 200 K at a rate of 10 K / min. The intensities for each irradiating energy were integrated and corrected for the spectral distribution of the irradiation light obtained with aid of yellow lumogen. The corrected spectra were normalized at 5.7 eV to minimize the influence of size variation of the samples. The edge of the excitation spectrum of TSL shows the threshold of the creation of separated electrons and holes in the crystal. The irradiating energy created charge carriers in the crystals which were accumulated at the change carrier traps present in the lattice. When the crystals were heated the trapped charge carriers were released and radiatively recombined giving rise to TSL. The result shows the shift of the threshold of electron-hole pair creation to lower energies with increasing Zn concentration similarly to the result obtained from excitation spectra measurements, and confirms the bandgap reduction in accordance with bandgap reduction in the sequence of studied solid solutions upon a gradual transition from $CdWO_4$ to $ZnWO_4$.

9. Summary

In the present work, cathodoluminescence, photostimulated and thermostimulated luminescence properties of solid solutions $Zn_xCd_{1-x}WO_4$ (x=0-1) were investigated by time-resolved luminescence spectroscopy method in the temperature range of 5.5-293 K. The main aim of the study was to reveal the changes in the mechanism of energy transfer to luminescence centers occurred due to the change of the ratio of zinc and cadmium cation concentrations in the solid solutions.

The following results were obtained:

- The measurements of emission spectra of $Zn_xCd_{1-x}WO_4$ solid solutions at low (12.2 and 78 K) and room temperature (RT) revealed the displacement in the position of the emission band towards lower wavelengths with changing Zn concentration (x value). The displacement barely detectable at low temperatures, but clearly observed at RT. Additionally, the widths of the emission band was found to be the largest at an average Zn concentration (x=0.5). The samples having low Zn content (x=0-0.3) showed an irregular displacement in the positions of the emission band at RT. The reason of the irregular shift in the position of the emission band was clarified by the studies emission decay kinetics.
- Decay curves of the excitonic emission were measured for all samples in the wavelength range 400 to 650 nm with a step of 25 nm. The decay kinetics was presented by two exponential components with decay times 15 μs and 28 μs, characteristic of $CdWO_4$ and $ZnWO_4$, respectively. The dependence of the ratio of integrated emission intensities of two components on x value revealed that exciton formation is highly favorable on WO_6 anion complexes having zinc in their surrounding in mixed crystals. The contribution of the emission of Zn-perturbed excitons in the total emission is relatively high even at low Zn concentrations, and because of this, a gradual shift in the emission band position with changing x value cannot be seen in $Zn_xCd_{1-x}WO_4$ solid solutions.
- Excitation spectra of the excitonic emission were measured at 12.2 K, 78 K and RT. The excitation spectra showed a gradual shift of excitation edge to a lower energy with an increase of Zn concentration in accordance with the fact that the bandgap of $ZnWO_4$ (4.6 eV) is smaller than that of $CdWO_4$ (4.98 eV). At 12.2 K, the onset of sample $Zn_{0.1}Cd_{0.9}WO_4$ appeared at ~ 4 eV, however, the onset of the same sample was

observed at 3.85 eV at RT, this shift in excitation edge was due to the electron-phonon interaction.

In the excitation spectra, a reverse onset shift was observed for the $ZnWO_4$ sample with respect to other studied samples. Such shift was not observed for a high-quality $ZnWO_4$ single crystal, which was also measured as a reference sample. This allowed to ascribe an unusual onset position of the excitation spectrum to structural imperfections and surface influence in the studied small-size crystals.

- Cathodoluminescence (CL) spectra of the selected samples with x=0.2, 0.3, 0.7, and 0.8 were also measured at 5.5 K with excitation energy of 10 keV. All samples showed maximum emission at 483 nm which is close to the $ZnWO_4$ emission wavelength. This observation supports the hypothesis that also excitons formed in the process of recombination of electron-hole pairs are mainly created near the zinc site.
- Thermostimulated luminescence (TSL) curves were measured for selected $Zn_xCd_{1-x}WO_4$ solid solutions upon the irradiation by UV photons or electron beam for 30 minutes. Two main broad peaks were observed near 90 and 140 K, whereas both showed a near-linear relation with the concentration of zinc in the samples, indicating that also the recombination of trapped charge carriers takes place preferentially near Zn cations. This was also confirmed by measuring the TSL spectra, which were centered at 480 nm for the peak corresponding to 140 K and 490 nm for the peak appeared at 90 K. TSL creation spectra also demonstrated a low energy shift at increasing Zn concentration in solid solution, in accordance with bandgap reduction upon a gradual transition from $CdWO_4$ to $ZnWO_4$.

9. Kokkuvõte

Käesolevas töös uuriti aeglahutusega spektroskoopia meetodiga temperatuuridel 5.5-293 K tahkete $Zn_xCd_{1-x}WO_4$ (x=0-1) lahuste katoodluminestsentsi ning foto- ja termostimuleeritud luminestsentsi omadusi. Uurimuse põhieesmärgiks oli välja selgitada, millised muutused toimuvad tahkete lahuste luminestsentstsentrile energia ülekande mehhanismis tsingi ja kaadmiumi katioonide kontsentratsiooni muutumisel.

Saadi järgmised tulemused:

- $Zn_xCd_{1-x}WO_4$ tahkete lahuste kiirgusspektrite uurimine madalal (12.2 and 78 K) ja toa temperatuuril ilmutasid lahuste kiirgusribade nihet väiksemate lainepikkuste poole Zn kontsentratsiooni (x väärtuse) suurenedes. See nihe on vaevumärgatav madalatel temperatuuridel, kuid selgesti vaadeldav toatemperatuuril. Kiirgusriba on kõige laiem keskmise tsingi kontsentratsiooni (x=0.5) puhul. Kiirgusriba nihe on ebakorrapärane, eriti proovides, kus tsingi sisaldus on väike (x=0-0.3). Sellise ebaregulaarse nihke põhjusi tuvastati tahkete lahuste kiirguse kustumiskineetika uurimisel.
- Kiirguse kustumiskõverad olid salvestatud lainepikkustel 400 kuni 600 nm sammuga 25 nm. Kõikide lahuste kiirguse kustumises leiti kaks komponenti kustumisajaga τ_1= 15 µs ja τ_2= 28 µs, mis on iseloomulikud vastavalt $CdWO_4$ ja $ZnWO_4$ kristallidele. Mõlema komponendi jaoks saadi integreeritud kiirguse spektrid, fikseerides τ_1 and τ_2 väärtusi. Kahe komponendi integraalsete intensiivsuste suhte sõltuvus x väärtusest näitas, et tahketes lahustes moodustuvad eksitonid eelistatult nende WO_6 anioonkompleksite kõrval, mis asuvad Zn võresõlme läheduses. Nimelt näitasid saadud spektrid, et Zn lisandamine $CdWO_4$ kristalli isegi minimaalsel kontsentratsioonil teeb mõlema komponendi panuse materjali kiirgusse võrreldavaks, mis seletab ka ebakorrapärasused, mis on täheldatud kiirgusriba nihkes.
- Ergastusspektrid mõõdeti tahkete lahuste eksitonkiirguse jaoks temperatuuridel 12.2 K, 78 K ja toatemperatuuril. Leiti, et tahkete lahuste kiirguse ergastusspektri äär nihkub järg-järguliselt madalamate energiate poole tsingi kontsentratsiooni suurenedes lahuses. Selline nihe on heas vastavuses keelutsooni kitsenemisega, kuna selle laius on 4.98 eV $CdWO_4$-s ja 4.6 eV $ZnWO_4$-s. Ergastusspektri äär $Zn_{0.1}Cd_{0.9}WO_4$ proovi jaoks nihkus uuritud ühendites ~ 4 eV juurest temperatuuril 12.2 K ja 3.85 eV-ni toatemperatuuril tugeva elektron-foonon vastasmõju tõttu.

$ZnWO_4$ (x=1) proovi ergastusspektri äär oli nihkes vastassuunas võrreldes teiste suure tsingi kontsentratsiooniga proovidega. Sellist nihet pole täheldatud kõrge kvaliteediga $ZnWO_4$ monokristalli jaoks, mida samuti uuriti referentsproovina. See asjaolu lubas siduda ebatavalise ääre nihet $ZnWO_4$ (x=1) proovis struktuursete ja pinnadefektidega, mida on hulgi väikese suurusega proovi kristallides.

- Katoodluminestsentsi spektreid mõõdeti valitud tahke lahuse proovide joaks (x=0.2, 0.3, 0.7, ja 0.8) temperatuuril 5.5 K ja ergastavate elektronide energiaga 10 eV. Kõikide provide kiirgusriba maksimum asus 483 nm juures, mis on lähedane $ZnWO_4$ kiirgus- riba asukohale. See tulemus kinnitas, et eksitonid, mis tekkivad tahketes lahustes elektron-aukude rekombinatsiooni käigus, moodustuvad samuti eelistatult tsingi võresõlme läheduses.
- Termostimuleeritud luminestsentsi (TSL) kõveraid mõõdeti valitud $Zn_xCd_{1-x}WO_4$ tahkete lahuste jaoks, eelnevalt 30 minuti jooksul UV footonitega või elektronkiirega kiiritatud kristallides. Kiritatud kristallide termostimuleeritud luminestsentsis tuvastati kaks põhilist laia piiki 90 ja 140 K juures, mis viitavad sellele, et tahketes lahustes domineerivad kaks põhilist laengukandjate lõksu. Nende piikide intensiivsuse peaaegu lineaarne sõltuvus tsingi kontsentratsioonist tõestab, et ka laengukandjate lõksustumine ja rekombinatsioon toimub tsingi võresõlme läheduses. Seda järeldust kinnitavad samuti TSL ribade spektraalsed asukohad, mis on 490 ja 480 nm, vastavalt, 90 ja 140 K piigi jaoks. Leiti samuti, et TSL ergastsuspektrite lävi nihkub madalamate energiate poole tsingi kontsentratsiooni kasvades, vastavalt keelutsoni kitsenemisele $CdWO_4$-st $ZnWO_4$-le siirdel.

Acknowledgements

I am profoundly grateful to my supervisor Drs. Vitali Nagirnyi and Nataliya Krutyak for their continuous support, patience and guidance provided during the whole period required to complete the present thesis. I would like to express my gratitude to the Head of Laboratory of Physics of Ionic Crystals Prof. Aleksandr Lushchik for allowing me to carry out my research in this laboratory. I am thankful to Prof. Marco Kirm, Dr. Dmitry Spassky, Dr. Eduard Feldbach and Dr. Ivo Romet for providing knowledge about spectroscopy and technical support in carrying out the measurements in at the Institute of Physics, University of Tartu on different setups.

I am also thankful to Dr. Boris Zadneprovski from All-Russian Research Institute for Synthesis of Materials, Alexandrov, Russia for synthesizing the crystals used for the measurements. Peeter Ritslaid from the Laboratory of Thin Films is thanked for XRF analysis of the samples and a gratitude also goes to Dr. Aile Tamm who organized the schedule of measurements.

I wish to thank all the personnel from the Laboratory of Physics of Ionic Crystals for friendly atmosphere, support and advices that helped me tremendously throughout the period. I am very thankful to my family and friends for their comprehensive support during my studies.

References

[1] M. Nikl, "Recent R&D Trends in Inorganic Single-Crystal Scintillator Materials for Radiation Detection," *Advanced optical materials,* vol. 3, pp. 463-481, 2015.

[2] C. Dujardin, "Needs, Trends, and Advances in," *IEEE TRANSACTIONS ON NUCLEAR SCIENCE,* vol. 65, no. 8, pp. 1977-1997, 2018.

[3] V. Nagirnyi, "Separation of excitonic and electron–hole processes in metal tungstates," *Journal of Luminescence,* Vols. 102-103, pp. 597-603, 2003.

[4] J. Zhang, "Structural investigation and scintillation properties of Cd1−xZnxWO4 solid solution single crystals," *CrystEngComm,* vol. 17, pp. 3503-3508, 2015.

[5] N. Krutyak, "Luminescent and structural properties of ZnxMg1-xWO4 mixed crystals," *Radiation Measurements,* vol. 90, pp. 43-46, 2016.

[6] A. Vasil'ev, "Relaxation of hot electronic excitations in scintillators: Account for scattering, track effects, complicated electronic structure," in *Proceedings of The Fifth International Conference on Inorganic Scintillators and Their Applications*, Moscow, 2000.

[7] Mikhail Korzhik, Gintautas Tamulaitis, Andrey N. Vasil'ev, Physics of Fast Processes in Scintillators (Particle Acceleration and Detection)., Springer, 2020.

[8] C. DUJARDIN, "Inorganic scintillating materials," *Électronique - Photonique | Optique Photonique,* 2018.

[9] P. Lecoq, Inorganic Scintillators for Detector Systems, Berlin: Springer, 2006.

[10] W. C. RÖNTGEN, "On a New Kind of Rays," *SCIENCE,* vol. 3, no. 59, pp. 227-231, 1896.

[11] F. Maddalena, L. Tjahjana, A. Z. Xie, S. W. Zeng, H. Wang, P. Coquet, W. Drozdowski, Christophe Dujardin, C. Dang, M. D. Birowosuto, "Inorganic, Organic, and Perovskite Halides with Nanotechnology for High-Light Yield X- and gamma-ray Scintillators," *MDPI Crystals,* vol. 9(2), no. 88, 2019.

[12] F. A. Kröger, Some aspects of the luminescence of solids., New York: Elsevier Pub. Co., 1948.

[13] H. D. KANG, "Large Size CdWO4 Crystal for Energetic X- and J-Ray Detection," *Journal of NUCLEAR SCIENCE and TECHNOLOGY,* vol. 45, no. 5, pp. 356-359, 2008.

[14] S. Izumi; S. Kamata; K. Satoh; H. Miyai, "High energy X-ray computed tomography for industrial applications.," *IEEE Transactions on Nuclear Science ,* vol. 40, no. 2, pp. 158 - 161, 1993.

[15] R. Deych, "Cadmium tungstate detector for computed tomography," in *Proceedings of the International Conference on Inorganic Scintillators and their Application*, Delft, 1995.

[16] M. Daturi, "Crystallographic and catalytic studies of a new solid solution CdMoxW1–xO4," *J. Chim. Phys.,* vol. 93, pp. 2043-2053, 1996.

[17] V. Atuchin, "Low Thermal Gradient Czochralski growth of large CdWO4 crystals," *Journal of Solid State Chemistry,* vol. 236, pp. 24-31, 2016.

[18] Y. Abraham, "Electronic structure and optical properties of CdMoO4 and CdWO4," *The American Physical Society,* vol. 62, no. 3, pp. 1733-1741, 2000.

[19] R. Laasner, "G0W0 band structure of CdWO4," *Journal of Physics: Condensed Matter,* vol. 26, no. 12, 2014.

[20] Tetsu Oi, "Scintillation study of ZnW04 single crystals," *Applied Physics Letters,* vol. 36, p. 278, 1980.

[21] H. G. Moser, "SCINTILLATION PROPERTIES OF ZnWO4," *Journal of Luminescence,* vol. 33, pp. 109 - 113, 1985.

[22] R. Bernabei, "Optical, luminescence, and scintillation properties of advanced ZnWO4 crystal scintillators," *Nuclear Inst. and Methods in Physics Research,* vol. 1029, 2022.

[23] Y. C. Zhu, J. G. Lu , Y. Y. Shao, H. S. Sun, J. Li, S. Y. Wang, B. Z. Dong, Z. P. Zheng, "Measurements of the scintillation properties of ZnWO4 crystals," *Nuclear Instruments and Methods in Physics Research,* vol. 244, no. 3, pp. 579-581, 1986.

[24] B. Grabmaier, "CRYSTAL SCINTILLATORS," *IEEE Transactions on Nuclear Science,* vol. 31, pp. 372 - 376, 1984.

[25] R. Bernabei, "Search for double beta decay of zinc and tungsten with low background ZnWO4 crystal scintillators," *Nuclear Physics,* vol. 826, pp. 256 - 273, 2009.

[26] H. Kraus, "ZnWO4 scintillators for cryogenic dark matter experiments," *Nuclear Instruments and Methods in Physics Research,* vol. 600, pp. 597 -598, 2009.

[27] O. Khyzhun, "Electronic properties of ZnWO4 based on ab initio FP-LAPW band-structure calculations and X-ray spectroscopy data," *Materials Chemistry and Physics,* vol. 140, no. 2 - 3, pp. 588 - 595, 2013.

[28] V. Kolobanov, "Optical and luminescent properties of anisotropic tungstate crystals," *Nuclear Instruments and Methods in Physics Research,* vol. 486, no. 1-2, pp. 496-503, 2002.

[29] M. A. Dahlborg, "Structural Changes in the System Zn1-xCdxWO4, Determined from Single Crystal Data," *Acta Chemica Scandinavica ,* vol. 53, pp. 1103-1109, 1999.

[30] D.Spassky, "Energy transfer in solid solutions ZnxMg1−xWO4," *Optical Materials,* vol. 36, no. 10, pp. 1660-1664, 2014.

[31] V. V. Atuchin, "Structural and Electronic Properties of ZnWO4(010) Cleaved Surface," *Crystal Growth & Design,* vol. 11, pp. 2479-2484, 2011.

Appendix

License

Non-exclusive licence to reproduce the thesis and make the thesis public

I, **Muhammad Usama Jamal**

1.grant the University of Tartu a free permit (non-exclusive licence) to

reproduce, for the purpose of preservation, including for adding to the DSpace digital archives until the expiry of the term of copyright, my thesis

Energy transfer processes in solid solutions $Zn_xCd_{1-x}WO_4$ supervised by **Dr. Vitaly Nagirnõi and Dr. Nataliya Krutyak**

2. I grant the University of Tartu a permit to make the thesis specified in point 1 available to the public via the web environment of the University of Tartu, including via the DSpace digital archives, under the Creative Commons licence CC BY NC ND 4.0, which allows, by giving appropriate credit to the author, to reproduce, distribute the work and communicate it to the public, and prohibits the creation of derivative works and any commercial use of the work until the expiry of the term of copyright.

3. I am aware of the fact that the author retains the rights specified in points 1 and 2.

4. I confirm that granting the non-exclusive licence does not infringe other persons' intellectual property rights or rights arising from the personal data protection legislation.

Muhammad Usama Jamal

31/05/2022